Cyclo(RGD)-Decorated Reduction-Responsive Nanogels Mediate Targeted Chemotherapy of Integrin Overexpressing Human Glioblastoma In Vivo

Wei Chen, Yan Zou, Zhiyuan Zhong, and Rainer Haag**

Dedicated to Prof. Kazunori Kataoka's 65th birthday

Cyclo(Arg-Gly-Asp) peptide (cRGD) decorated disulfide (SS) containing poly(vinyl alcohol) nanogels (cRGD-SS-NGs) with an average diameter of 142 nm prepared by inverse nanoprecipitation, "click" reaction, and cRGD conjugation are developed for targeted treatment of integrin overexpressing human glioblastoma in vivo. Doxorubicin (DOX) release from cRGD-SS-NGs is highly inhibited under physiological conditions, while accelerated at endosomal pH and in response to cytoplasmic concentration of glutathione. Confocal microscopy shows that cRGD-SS-NGs facilitate the cellular uptake and intracellular DOX release in $\alpha_v\beta_3$ integrin overexpressing human glioblastoma U87-MG cells. DOX-loaded cRGD-SS-NGs present much better killing activity toward U87-MG cells than that for nontargeted nanogels determined by MTT assay. The in vivo imaging and biodistribution studies reveal that DOX-loaded cRGD-SS-NGs have a much better tumor targetability toward human U87-MG glioblastoma xenograft in nude mice. Also the tumor growth is effectively inhibited by treatment with DOX-loaded cRGD-SS-NGs, while continuous tumor growth is observed for mice treated with nondecorated nanogels as well as free DOX. Furthermore, the treatment with DOX-loaded cRGD-SS-NGs has much fewer side effects, rendering these nanogels as a new platform for cancer chemotherapy in vivo.

1. Introduction

Advanced nanosystems for controlled drug delivery have received tremendous attention because these nanosystems confer prolonged circulation time, efficient tumor-targeted accumulation via the enhanced permeability and retention (EPR) effect, reduced side effects, and improved drug tolerance.[1] Owing to the impressive progress in materials science, various types of biocompatible nanocarriers, including liposomes, polymeric nanoparticles, micelles, and nanogels, have been developed for in vitro and in vivo drug delivery to meet the pharmaceutical requirements. Compared to other nanosystems, nanogels with internally cross-linked 3D structures are able to stably encapsulate bioactive compounds such as drugs, peptides/proteins, and DNA/RNA in their polymeric networks; moreover, nanogels actively participate in the drug delivery process due to their intrinsic properties like stimuli-responsive behavior, swelling, and softness, to achieve a controlled drug release at the target site.[2]

The use of stimuli-responsive nanogels in drug delivery has appeared as one of the most promising approaches in nanomedicine[3] because these nanogels are highly stable in protecting the drugs for prolonged blood circulation due

Dr. W. Chen, Prof. R. Haag
Institute of Chemistry and Biochemistry
Freie Universität Berlin
Takustrasse 3, Berlin 14195, Germany
E-mail: haag@chemie.fu-berlin.de
Dr. Y. Zou, Prof. Z. Y. Zhong
Biomedical Polymers Laboratory, and Jiangsu Key Laboratory of Advanced Functional Polymer Design and Application
Department of Polymer Science and Engineering
College of Chemistry
Chemical Engineering and Materials Science
Soochow University
Suzhou 215123, P. R. China
E-mail: zyzhong@suda.edu.cn

DOI: 10.1002/smll.201601997

to their chemically cross-linked structure. Furthermore, the release profile can be modulated in response to external or internal signals, particularly to intracellular endosomal/lysosomal pH (4.5–6.0) and cytoplasmic glutathione (GSH, 0.5×10^{-3}–10×10^{-3} M).[4] It should be noted that nanogels with dual and multistimuli responses have shown unprecedented control over drug delivery and thus led to superior in vitro and/or in vivo anticancer efficacy, whereby these combinational responses take place either simultaneously or in a sequential manner at the pathological site.[5]

Poly(vinyl alcohol) (PVA), which has been approved by the Food and Drug Administration (FDA) for good biocompatibility, has been widely applied in biomedical area such as protein/enzyme immobilization, and cell encapsulation in the form of micro/hydrogel materials.[6] However, PVA nanostructures failed to meet the demand, especially in the field of nanomedicine area, due to their inhomogeneous interior, high porosity, low drug affinity, and uncontrollable release behavior. Although the traditional PVA nanocarriers lit with nonfouling shielding can enhance the accumulation by EPR effect in tumor tissues, inefficient uptake at tumor sites and into tumor cells will decrease the therapeutic effect of the administered drug dose, and nonspecific spreading to healthy tissues will lead to serious side effects. We previously reported charge-conversional, reducible PVA nanogels for enhanced cellular uptake toward universal tumor cells and efficient intracellular drug release; however, these ultra pH-sensitive linkers could not sustain for a long time even at physiological conditions (pH 7.4).[7] Nanogel surface decorated with a specific tumor-homing ligand can largely increase retention and accumulation in the tumor vasculature as well as provide a selective and efficient internalization by target tumor cells.[8] It has been demonstrated that cRGD has a high affinity with the $\alpha_v\beta_3$ integrin receptors overexpressed on angiogenic endothelial cells and tumor cells such as malignant glioma cells, breast cancer cells, bladder cancer cells, and prostate cancer cells, which render cRGD a unique molecular ligand for targeted cancer chemotherapy.[9] Therefore, we designed cRGD-decorated reduction-responsive PVA nanogels for investigating targeted chemotherapy of human glioblastoma in vivo (**Scheme 1**). Besides the advantages of nondecorated PVA nanogels—defined shape and size, high loading of anticancer drug, inhibited premature drug release, and efficient intracellular drug release—these cRGD-decorated nanogels can be well recognized and taken up by glioblastoma cells via receptor-mediated endocytosis, enhancing the tumor penetration and antitumor activity. Using these nanogels, the targetability and cytotoxicity toward human glioblastoma U87-MG cells, pharmacokinetics, and biodistribution in vivo, as well as therapeutic effects on human glioblastoma xenografts in mice, were investigated and the results were compared with those obtained using nondecorated reducible or unreducible counterparts.

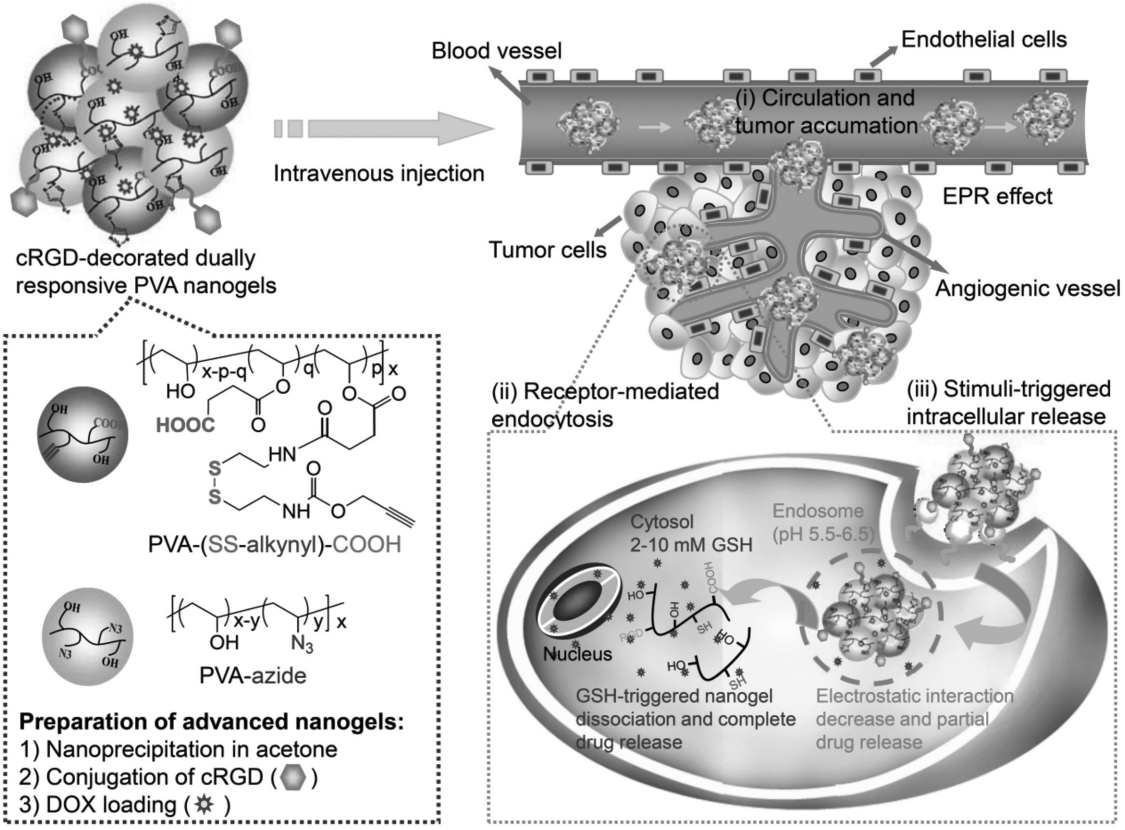

Scheme 1. Illustration of cRGD-decorated reduction-responsive PVA nanogels (cRGD-SS-NGs) for active integrin-targeting and efficient treatment of human glioblastoma. These cRGD-SS-NGs give (i) super stability for circulation and tumor accumulation, (ii) enhanced cellular uptake via receptor-mediated endocytosis, and (iii) pH and reduction-triggered intracellular drug release, resulting in potent antitumor effect.

2. Results and Discussion

2.1. Formation and Reduction-Sensitivity of cRGD-Decorated Nanogels

Reduction-sensitive and insensitive PVA nanogels (SS-NGs and NSS-NGs) based on carboxyl/alkynyl-functionalized and azido-functionalized PVA were prepared by nanoprecipitation in acetone via a "click" reaction using propargyl alcohol as a terminator.[7] cRGD peptide was subsequently conjugated to SS-NGs by carbodiimide chemistry using the amino group of cRGD peptide and the carboxyl group of nanogels to prepare cRGD-decorated reducible nanogels (cRGD-SS-NGs). The content of the cRGD moiety on cRGD-SS-NGs was ≈1.5 wt%, as determined by the Micro bicinchoninic acid (BCA) protein assay. cRGD-SS-NGs with an average size of 142 nm were determined by dynamic light scattering (DLS) and transmission electron microscopy (TEM) (**Figure 1**a). The size of cRGD-SS-NGs was slightly larger than that of SS-NGs (132 nm) and NSS-NGs (120 nm). The reduction-sensitivity of cRGD-SS-NGs was studied by using DLS to monitor the nanogels' size over time in response to 10×10^{-3} M GSH. It was discovered that cRGD-SS-NGs quickly dissociated with a 50 nm decrease in 1 h, and that the nanogel size further reduced to 40 nm in 6 h (Figure 1b), while little size change was detected for the cRGD-SS-NGs within 24 h in the absence of GSH. It is therefore evident that the reduction-sensitivity of cRGD-SS-NGs was not altered after the cRGD conjugation.

2.2. Loading and Triggered Release of DOX

Doxorubicin (DOX) loading into cRGD-SS-NGs proceeded after cRGD-conjugation onto the SS-NGs. Due to the electrostatic and hydrophobic interactions, DOX was efficiently entrapped in the cRGD-SS-NG networks with drug loading efficiency (DLE) of 65.4% and 58.6% at theoretical drug loading contents (DLC) of 5 and 10 wt%, respectively. The DOX loading capability of cRGD-SS-NGs is comparable with that of SS-NGs and NSS-NGs (Table S1, Supporting Information). The in vitro release profile of DOX from cRGD-SS-NGs was investigated at 37 °C in the following four media: pH 7.4, pH 5.5, pH 7.4, with 10×10^{-3} M GSH, and pH 5.5 for 4 h followed by pH 7.4 with 10×10^{-3} M GSH. DOX release at physiological pH (pH 7.4) was highly restricted with a released amount of ≈20% after 48 h. Attributed to the better solubility and the decrease of the electrostatic interaction at the lower pH condition, DOX release was accelerated with 65% of DOX released at pH 5.5 within 48 h (Figure 1c). The DOX release was also accelerated under a reducing environment containing 10×10^{-3} M GSH at pH 7.4 due to the cleavage of disulfide bond, in which 61% of DOX was released in 48 h. Interestingly, it was found that DOX release was more efficient in an intracellular-mimicking pathway: at endosomal/lysosomal pH (pH 5.5) for 4 h, and then in cytoplasmic reducing conditions (pH 7.4 with 10×10^{-3} M GSH). Similar DOX release tendency was also observed for SS-NGs.[7] DOX release from cRGD-SS-NGs clearly proceeds in a controlled manner and can be activated by a synergistic trigger of low pH and reduction environments.

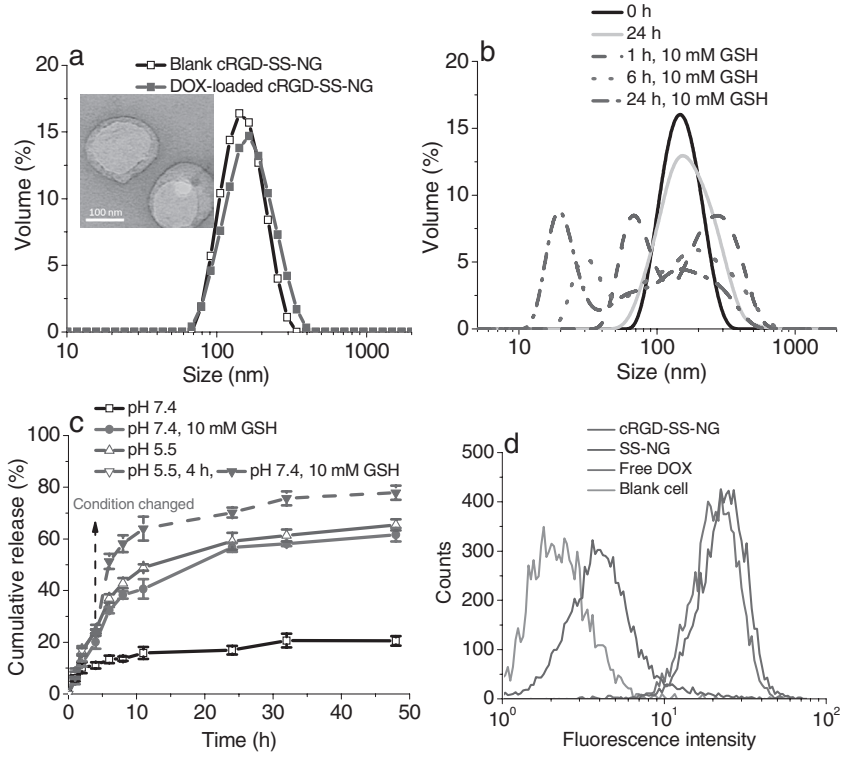

Figure 1. a) Size distribution of blank and DOX-loaded cRGD-decorated PVA nanogels (cRGD-SS-NGs) determined by DLS (inlet: TEM image of cRGD-SS-NG). b) Size changes of cRGD-SS-NGs in response to 10×10^{-3} M GSH followed by DLS. c) pH or GSH-triggered release of DOX from cRGD-SS-NGs at 37 °C at pH 7.4 or 5.5, and DOX release from cRGD-SS-NGs at pH 5.0 for 4 h followed by pH 7.4 and 10×10^{-3} M GSH, mimicking the intracellular trafficking pathway. d) Flow cytometry profiles of U87-MG cells after 1 h incubation with DOX-conjugated PVA nanogels and free DOX at a DOX dosage of 5.0 μg mL^{-1} (U87-MG cells without any treatment were used as a blank control).

2.3. Cellular Uptake and Intracellular Release of DOX

To demonstrate that cRGD-decorated nanogels can be more efficiently internalized by cells via $\alpha_v\beta_3$ integrin receptor-mediated endocytosis, we investigated the cellular uptake behavior of DOX-conjugated cRGD-SS-NGs and SS-NGs using U87-MG cells. After just 0.5 h incubation, cRGD-SS-NGs started to internalize with the cells and distribute in the cytoplasm. They intensively overlaid with the endosomes after 1 h incubation (Figure S1, Supporting Information). However, the internalization of SS-NGs was relatively slow with very weak DOX

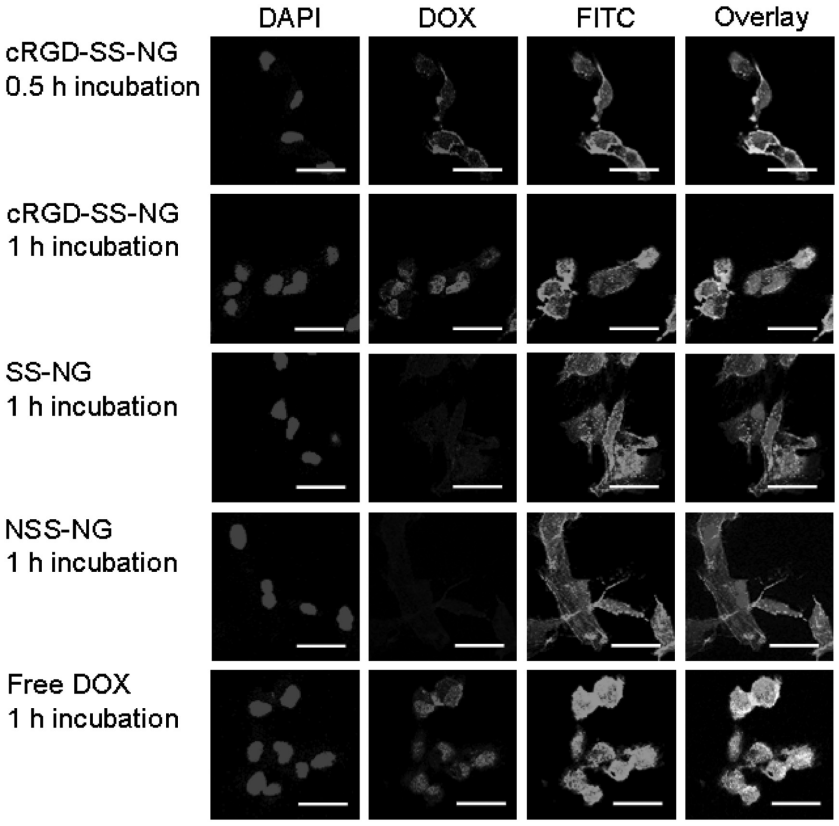

Figure 2. CLSM images of U87-MG cells after 0.5 or 1 h incubation with DOX-loaded PVA nanogels and free DOX. The DOX dosage was set as 5.0 μg mL^{-1}. The images show for each panel from left to right cell nuclei stained by DAPI (blue), DOX fluorescence in cells (red), cytoskeleton labeled by phalloidin-FITC (green), and overlays of three images. The scale bars correspond to 25 μm in all the images.

fluorescence found inside the cells. Cellular uptake of DOX-conjugated nanogels was further quantified by flow cytometry analysis. As expected, the flow cytometry result showed that U87-MG cells following 1 h treatment with cRGD-SS-NGs displayed greatly enhanced DOX fluorescence, much higher than that of cells incubated with SS-NGs under otherwise the same conditions (Figure 1d). We further investigated the intracellular DOX release from DOX-loaded nanogels in U87-MG cells using confocal laser scanning microscope (CLSM). Interestingly, significant DOX fluorescence was observed in the cytoplasm and peri-nuclei region of U87-MG cells with just 0.5 h incubation with cRGD-SS-NGs, and the released DOX quickly internalized with cell nuclei in 1 h incubation time, which was notably similar to U87-MG cells following 1 h incubation with free DOX (**Figure 2**). In contrast, weak and little DOX fluorescence was found inside the cells incubated for 1 h with DOX-loaded SS-NGs and NSS-NGs, respectively. The low DOX release from SS-NGs found inside the cells was mainly attributed to the inefficient cellular uptake, while the lowest DOX release of NSS-NGs inside cells was mainly due to both the inefficient cellular uptake and the restricted intracellular release. These results prove that cRGD-SS-NGs mediate more efficient cellular uptake and intracellular anticancer drug release than SS-NGs and NSS-NGs, mostly due to the combination of receptor-mediated endocytosis and synergistic pH/reduction dual-stimuli.

2.4. Cytotoxicity of DOX-Loaded Nanogels

MTT assays in U87-MG cells revealed that all three types of blank nanogels (cRGD-SS-NGs, SS-NGs, and NSS-NGs) were practically nontoxic (cell viabilities ≥ 90%) up to a tested concentration of 1.0 mg mL^{-1} (**Figure 3**a), which confirmed that these PVA-based nanogels had good biocompatibility. DOX-loaded nanogels, however, displayed different levels of cell killing activity toward U87-MG cells after 4 h treatment with different nanogel samples. Importantly, U87-MG cells treated with DOX-loaded cRGD-SS-NGs displayed a lower IC_{50} (half inhibitory concentration) of 1.63 μg DOX equiv. mL^{-1} than those incubated with DOX-loaded SS-NGs as well as NSS-NGs under otherwise the same conditions, which had the IC_{50} values of 6.62 and 18.46 μg DOX equiv. mL^{-1}, respectively (Figure 3b). This higher cell killing activity of cRGD-SS-NGs is in accordance with the CLSM observations that cRGD-SS-NGs mediated a faster uptake and better intracellular drug release than the corresponding SS-NGs and NSS-NGs (Figure 2). It should be noted that, although free DOX had the lowest IC_{50} value (1.11 μg DOX equiv. mL^{-1}) in the cell test, the strong side effects of free DOX should be considered for in vivo tests. From the in vitro tests, we can conclude that cRGD-SS-NGs could facilitate efficient cellular uptake and intracellular drug delivery to achieve remarkable cell killing activity.

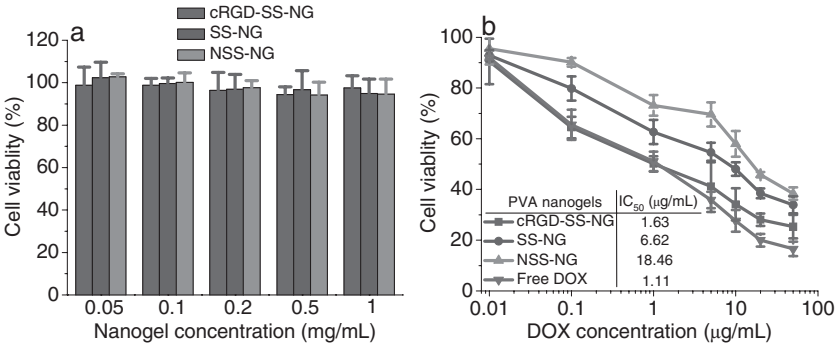

Figure 3. Cytotoxicity of PVA nanogels determined by MTT assay using U87-MG cells. a) Cytotoxicity of bare PVA nanogels after 48 h incubation. b) Cytotoxicity of DOX-loaded PVA nanogels and free DOX (the cells were treated with DOX-loaded PVA nanogels or free DOX for the first 4 h, then the medium was removed and replenished with fresh culture medium for another 48 h culture).

2.5. In Vivo Pharmacokinetics and Imaging Studies

In the following in vivo study, we first investigated the in vivo pharmacokinetics of DOX-loaded nanogels in nude mice. The plasma levels of DOX were determined by fluorescence spectroscopy at different time intervals following a single intravenous (i.v.) injection of DOX-loaded nanogels or free DOX (10 mg DOX equiv. kg^{-1}). Notably, DOX assisted by three types of nanogels revealed a significantly longer circulation time than free DOX, in which the concentration of DOX in plasma decreased to undetectable levels in 4 h after injection of free DOX, while a considerable amount of DOX was found even after 24 h following administration of DOX-loaded nanogels (**Figure 4**a). To examine the biodistribution of released DOX in tumor-bearing mice, the ex vivo fluorescence images of tumors and major organs including heart, liver, spleen, lung, and kidney were taken following 8 h i.v. injection of DOX-loaded nanogels or free DOX. The ex vivo fluorescence images revealed that mice treated with DOX-loaded cRGD-SS-NGs had strong DOX fluorescence in the tumor (Figure 4b), which showed significantly higher intensity than other treatment groups. The amount of DOX accumulated in tumors and major organs were further quantified by fluorometry. It is remarkable to note that cRGD-SS-NGs showed much better tumor targetability compared to nanogels without cRGD decoration or free DOX. The tumor uptake of DOX was 5.54% of injected dose per gram of tissue (% ID g^{-1}) for cRGD-SS-NGs, which was about 2, 4.5, and 8 times higher than for SS-NGs, NSS-NGs, and free DOX, respectively (Figure 4c). This tumor uptake of DOX for cRGD-SS-NGs is comparable to or higher than that of cRGD-decorated NIR-responsive gold-nanorod/poly(ethylene glycol)-polycaprolactone (AuNR/PEG–PCL) hybrid nanoparticles[10] as well as choline derivate-modified pegylated DOX prodrug[11] for in vivo glioblastoma therapy. Moreover, cRGD-SS-NGs displayed reduced accumulation in normal tissues, such as heart, liver, spleen, lung, and kidney, as compared with nondecorated SS-NGs and NSS-NGs. The tumor-to-normal tissue (T/N) distribution ratios of DOX demonstrated that cRGD-SS-NGs could in general reduce DOX uptake by healthy organs or tissues while largely increase DOX accumulation in the glioblastoma tumors (Figure 4d).

To obviously evaluate the in vivo tumor-targetability of nanogels, 1,1′-dioctadecyltetramethyl indotricarbocyanine iodide (DIR)-loaded nanogels were injected intravenously to nude mice bearing U87-MG human glioblastoma tumor xenografts and monitored using a near-infrared fluorescence imaging system at excitation of 747 nm and emission of 774 nm. As shown in **Figure 5**, cRGD-SS-NGs exhibited much higher DIR fluorescence in the tumor tissues compared to SS-NGs and NSS-NGs. For example, eight hours after injection, DIR fluorescence accumulated more in the tumor tissue for cRGD-SS-NGs, as compared to that for nondecorated

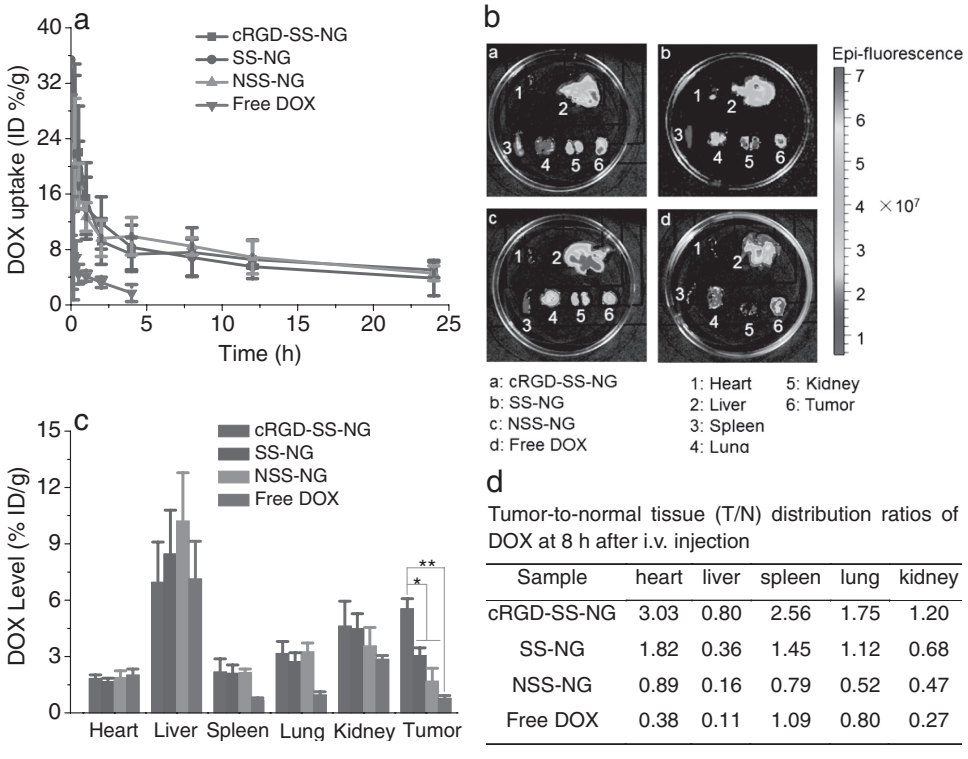

d

Tumor-to-normal tissue (T/N) distribution ratios of DOX at 8 h after i.v. injection

Sample	heart	liver	spleen	lung	kidney
cRGD-SS-NG	3.03	0.80	2.56	1.75	1.20
SS-NG	1.82	0.36	1.45	1.12	0.68
NSS-NG	0.89	0.16	0.79	0.52	0.47
Free DOX	0.38	0.11	1.09	0.80	0.27

Figure 4. a) In vivo pharmacokinetics of DOX-loaded PVA nanogels and free DOX in nude mice (DOX uptake was expressed as injected dose per gram of tissue (% ID g^{-1}) estimated by fluorescence spectroscopy). b) Ex vivo fluorescence images of organs and tumors from the U87-MG human glioblastoma-bearing nude mice following 8 h postintravenous injection. c) In vivo biodistribution of DOX-loaded PVA nanogels and free DOX in the tumor bearing nude mice at 8 h postintravenous injection quantified by fluorescence spectroscopy (DOX level uptake was expressed as injected dose per gram of tissue). d) Estimation of tumor-to-normal tissue (T/N) distribution ratios of DOX at 8 h after i.v. injection. All the data are presented as the average ± standard deviation ($n = 3$, student's t-test: $^*p < 0.05$, $^{**}p < 0.01$).

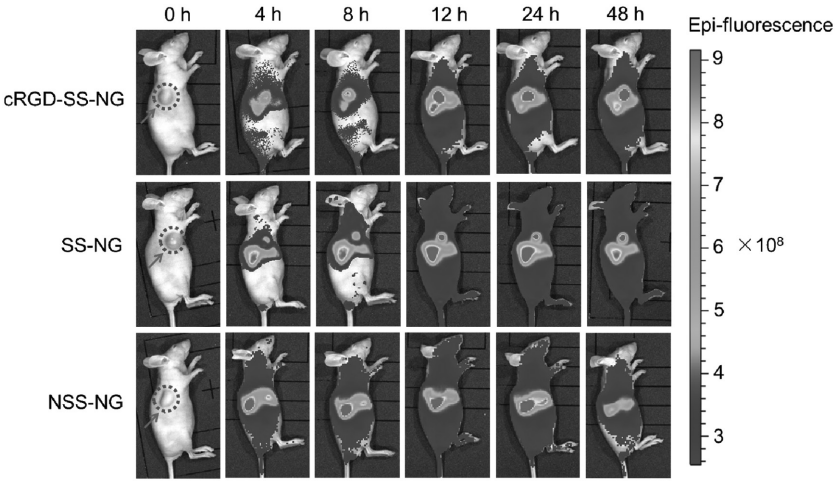

Figure 5. In vivo fluorescence images of U87-MG human glioblastoma tumor xenograft bearing nude mice at different time points following injection of DIR-loaded PVA nanogels (DIR concentration: 20 μg mL^{-1}). The images were acquired and analyzed using Lumia II software.

nanogels, especially for nondecorated reduction-insensitive NSS-NGs, in which most of DIR fluorescence presented in the liver (Figure 5). This observation is in accordance with the ex vivo result (Figure 4b,c). It was found that the tumor targetability was further improved as the time increased, in which much stronger DIR fluorescence was observed in the tumor tissue using cRGD-SS-NGs in 48 h after injection, compared with that for SS-NGs and NSS-NGs. It is demonstrated that cRGD-SS-NGs exhibit excellent tumor targetability to glioblastoma.

2.6. In Vivo Therapeutic Efficacy of DOX-Loaded Nanogels

The therapeutic performance of DOX-loaded nanogels was evaluated using U87-MG human glioblastoma tumor-bearing nude mice. As tumors grew to about 30–50 mm^3 in volume, mice were treated with DOX-loaded nanogels and free DOX (7.5 mg DOX equiv. kg^{-1}) by i.v. injection, and mice treated with phosphate buffered saline (PBS) were used as control. The treatment was repeated every three days. The results showed that tumor growth was effectively inhibited by DOX-loaded cRGD-SS-NGs, while continuous tumor growth was observed for mice treated with DOX-loaded SS-NGs and NSS-NGs (**Figure 6**a). The relative tumor volume at 12 d was 0.75, 3.36, and 5.30 for mice treated with DOX-loaded cRGD-SS-NGs, SS-NGs, and NSS-NGs, respectively. For the nanogels without cRGD decoration, the antitumor activity was more efficient using reduction-sensitive SS-NGs than with reduction-insensitive NSS-NGs, which was mainly due to reduction-triggered, intracellular drug delivery. Even for the treatment with free DOX, the relative tumor volume of the mice was still up to 2.79, which was much larger than when treated with cRGD-SS-NGs. These results demonstrated that both cRGD peptide targeting and reduction triggered drug release played a highly important role for effective tumor inhibition (cRGD-SS-NG vs SS-NG and SS-NG vs NSS-NG). In addition, mice treated with DOX-loaded nanogels or PBS had little change of body weights, which was in sharp contrast to ≈20% body weight loss for mice treated with free DOX (Figure 6b), indicating that DOX assisted by nanogel carriers (cRGD-SS-NG, SS-NG, and NSS-NG) has little systemic toxicity. The photographs of tumor blocks isolated at day 12 also obviously showed that mice treated with DOX-loaded cRGD-SS-NGs had much smaller tumor sizes as compared to the treatment with SS-NGs and NSS-NGs, and even smaller than the treatment with free DOX (Figure 6c). The histological analysis using

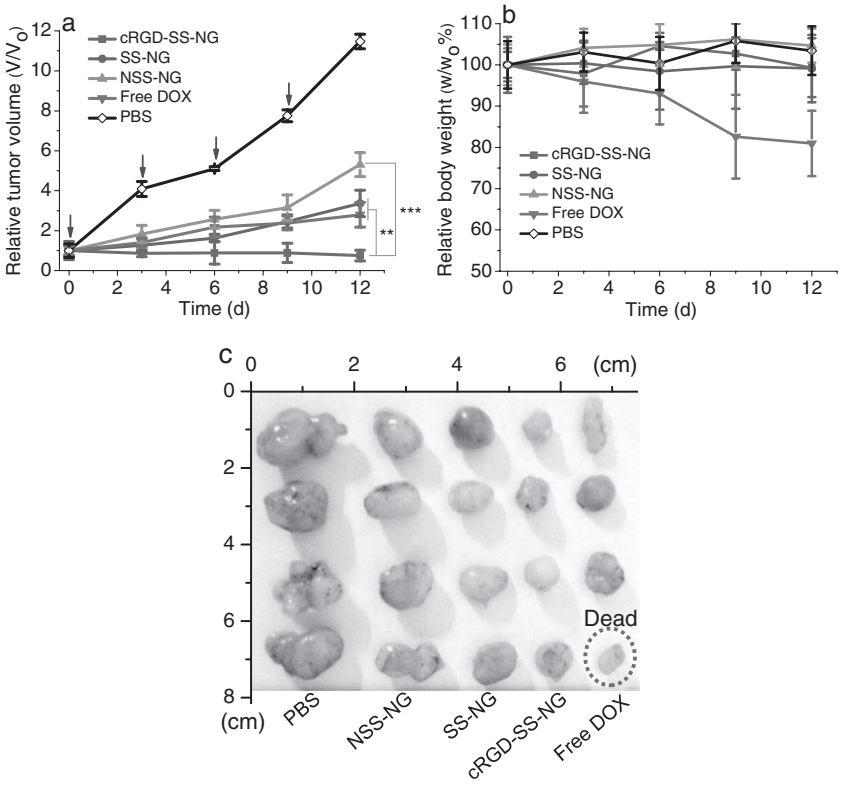

Figure 6. In vivo antitumor performance of DOX-loaded PVA nanogels in U87-MG human glioblastoma tumor xenograft bearing nude mice. The drug was given on days 0, 3, 6, and 9 at a DOX dosage of 7.5 mg equiv. per kg body weight in 0.2 mL PBS. a) Tumor volume changes of mice treated with DOX-loaded cRGD-SS-NGs, SS-NGs, NSS-NGs, free DOX, and PBS, respectively. b) Body weight changes of mice in different treatment groups within 12 d. c) Photographs of tumor blocks collected from the mice with different treatments on day 12 (the tumor block marked with red ring was collected from a dead mouse treated with free DOX). Data are presented as the average ± SD ($n = 4$, student's t-test: $^{**}p < 0.01$, $^{***}p < 0.001$).

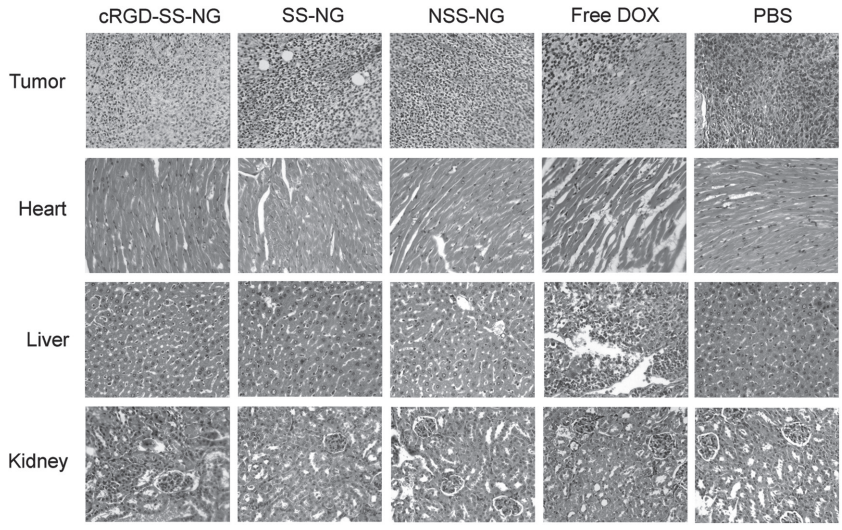

Figure 7. H&E-stained tumor, heart, liver, and kidney sections excised from U87-MG human glioblastoma tumor xenograft bearing nude mice following 12 d different treatments (the images were observed by an Olympus BX41 microscope at a magnification of 400).

hematoxylin and eosin (H&E) staining revealed that DOX-loaded cRGD-SS-NGs caused more necrosis in the tumor tissue compared to the groups treated with SS-NGs and NSS-NGs (**Figure 7**). It should be further noted that using cRGD-SS-NGs had less damage to liver and heart than with SS-NGs and NSS-NGs because of the cRGD-induced tumor targeting, which is in accord with the observation of NIR fluorescence images using DIR-loaded nanogels (Figure 5). Although tumor necrosis was also observed for the mice treated with free DOX, the damage of heart and liver tissues treated with free DOX indicated failure of cardiac myocytes and infiltration of inflammatory cells, which showed much stronger side effects than that with DOX-loaded nanogels. Therefore, the DOX-loaded cRGD-SS-NGs possess a significantly better therapeutic effect toward U87-MG human glioblastoma tumor xenografts in mice compared to SS-NGs, NSS-NGs, and free DOX.

3. Conclusion

In summary, this is the first demonstration that cRGD-decorated, reduction-responsive nanogels (cRGD-SS-NGs), based on the FDA-approved PVA, afford a tumor-targeted and reduction-triggered intracellular release of DOX into human glioblastoma xenografts in mice, which results in efficient inhibition of tumor growth with little adverse effect. These multifunctional biocompatible nanogels with well-defined structure and size had excellent colloidal stability with only little drug leakage under physiological conditions and rapidly dissociated with triggered drug release at intracellular acidic and reductive conditions. They exhibited enhanced internalization in $\alpha_v\beta_3$ integrin overexpressed glioblastoma cells via the receptor-mediated endocytosis to induce the death of cancer cells compared to the nondecorated nanogel counterparts. These cRGD-decorated, reducible PVA nanogel systems present a promising platform for targeted and efficient cancer chemotherapy of $\alpha_v\beta_3$ integrin overexpressed malignant tumors in vivo. Furthermore, reducible PVA nanogels are highly versatile and can be possibly used for the delivery of various drugs and proteins to actively treat different malignant tumors with a specific targeting ligand decoration.

4. Experimental Section

Materials: 1-ethyl-3-(3-dimethylaminopropyl) carbodiimide (EDC, Acros, 97%), N-hydroxysuccinimide (NHS, Acros, 98%), L-GSH reduced (Sigma-Aldrich, >98%), doxorubicin hydrochloride (DOX·HCl, Sigma, 98%), DIR (AAT BioQuest Company), and fluorescein isothiocyanatelabeled phalloidin (phalloidin-FITC, Sigma) were used as received. Cyclo(Arg-Gly-Asp-Phe-Lys) (cRGD, > 95%) was purchased from Peptide Protein Research Ltd (United Kingdom). PVA (Mowiol 3–97, M_w = 16000 g mol^{-1}) was kindly provided by Kuraray Europe GmbH (Germany). Carboxyl-(cystamine-alkynyl)-functionalized PVA (PVA-COOH-(SS-alkynyl)) and azido-functionalized PVA (PVA-N_3) as well as the reduction-sensitive nanogels (SS-NGs) and reduction-insensitive nanogels (NSS-NGs) were prepared according to the previous report. For cell culture experiments, U-87 MG cells (Sigma) were cultured in Eagle's minimal essential medium (EMEM) with 2×10^{-3} M glutamine, 1% nonessential amino acids, 1×10^{-3} M sodium pyruvate (NaP) and 10% fetal bovine serum (FBS).

Preparation of cRGD-Decorated Reduction-Sensitive Nanogels (cRGD-SS-NGs): cRGD (10.0 mg, 0.017 mmol), EDC (4.0 mg, 0.020 mmol), and NHS (2.5 mg, 0.020 mmol) were added into 50 mL of SS-NG aqueous suspension (10 mg mL^{-1}), and the mixture was stirred at room temperature overnight. cRGD-SS-NGs were purified by dialysis in Milli-Q-water with a molecular weight cut off (MWCO) of 2000 and collected by freeze-drying. The content of cRGD moiety on the nanogels was determined by the Micro BCA protein assay kit. The nanogel samples were redispersed in phosphate buffer (PB, pH 7.4, 10×10^{-3} M) by sonication and characterized by DLS (Zetasizer Nano-ZS from Malvern Instruments equipped with a 633 nm He–Ne laser) and TEM.

Reduction-Sensitivity of cRGD-SS-NG: cRGD-SS-NG suspension (1.0 mg mL^{-1}) was divided into two aliquots of 1 mL and 10 µL of GSH solution (1.0 M) was added into one of the two aliquots with a final GSH concentration of 10×10^{-3} M. The samples were slowly shaken at 37 °C under an argon atmosphere protection, and the nanogel size was monitored over time by DLS.

DOX Encapsulation and In Vitro Release of cRGD-SS-NGs: To prepare DOX-loaded cRGD-SS-NGs, 2 mL of DOX·HCl solution in Milli-Q-water (5.0 mg mL^{-1}) was added into 45 mL of cRGD-SS-NG suspension (2.0 mg mL^{-1}), and the mixture were drastically stirred at room temperature for 0.5 h. The free drug was removed by glucan gel column chromatography (Sephadex G-25 Superfine). DLC and DLE were calculated according to the following formula: DLC (wt%) = (weight of loaded drug/total weight of polymer and loaded drug) × 100%; DLE(%) = (weight of loaded drug/weight of drug in feed) × 100%.

The in vitro release of DOX from cRGD-SS-NGs was investigated at 37 °C under following different conditions: (i) PB (10×10^{-3} M, pH 7.4), (ii) acetate buffer (10×10^{-3} M, pH 5.5), (iii) PB (10×10^{-3} M, pH 7.4) containing 10×10^{-3} M GSH, and (iv) acetate buffer (10×10^{-3} M, pH 5.5) first for 4 h, followed in PB (10×10^{-3} M, pH 7.4) containing 10×10^{-3} M GSH. DOX-loaded cRGD-SS-NG suspension was divided into four aliquots of 1 mL, and immediately transferred to a dialysis tube with a MWCO of 12 000–14 000. The dialysis tubes were immersed into 20 mL of appropriate buffers and shaken at 37 °C. At set time intervals, 5.0 mL of the release medium was taken out from each experimental group and replenished with an equal volume of fresh appropriate medium. To avoid oxidation of GSH, the release media were perfused with argon gas. To determine the amount of released DOX, calibration curves were run with DOX in buffer with different DOX concentrations according to the fluorescence spectra at the emission of 480 nm. To determine the drug loading content, the freeze-dried DOX-loaded nanogel samples were suspended in DMSO, and analyzed with UV spectroscopy. A calibration curve was obtained using DOX/DMSO solutions with different DOX concentrations. Release experiments were conducted in triplicate. The results are presented as the average ± standard deviation.

Cellular Uptake of DOX-Conjugated PVA Nanogels: DOX was linked to PVA-COOH-(SS-alkynyl) using a carbodiimide chemistry via the amino group of DOX and the carboxyl group of the polymer, and DOX-conjugated nanogels were also prepared by nanoprecipitation in acetone using propargyl alcohol as a terminator. After that, cRGD peptide was linked to DOX-conjugated nanogels also by carbodiimide chemistry to prepare cRGD-decorated DOX-conjugated nanogels. U87-MG cells were plated on microscope slides in a 24-well plate (1.0×10^4 cells per well) using EMEM culture medium containing 10% FBS. After 24 h incubation, the medium was replaced by 450 µL of fresh culture medium and 50 µL of prescribed amounts of DOX-conjugated nanogel samples or free DOX. After incubation for 0.5 and 1 h, respectively, the culture medium was removed and the cells were washed twice with PBS. The cells were fixed with 4% paraformaldehyde for 20 min, incubated with early endosomes antibody-FITC (Invitrogen, Germany) at 37 °C for 1 h, and the cell nuclei were stained with DAPI. Fluorescence images of cells were obtained with CLSM (Leica, Germany) and analyzed by Leica 2.6.0 software.

Cellular uptake of DOX-conjugated PVA nanogels was also quantified by flow cytometry analysis. U87-MG cells were cultured in a 12-well plate (1.0×10^5 cells per well) for 24 h, and then the medium was replaced by 900 µL of fresh culture medium and 100 µL of prescribed amounts of DOX-conjugated nanogel samples or free DOX. After 1 h incubation, the culture medium was removed, and the cells were rinsed thrice with PBS and treated with trypsin. Cells were fixed with 4% paraformaldehyde and resuspended in PBS supplemented with 1% fetal calf serum and 0.1% sodium azide. The quantification of fluorescence was performed by a FACScalibur (Becton Dickinson, Heidelberg, Germany).

Intracellular DOX Release from PVA Nanogels: U87-MG cells were plated on microscope slides in a 24-well plate (1.0×10^4 cells per well) using EMEM culture medium containing 10% FBS. After 24 h incubation, the medium was replaced by 450 µL of fresh culture medium and 50 µL of prescribed amounts of DOX-loaded nanogel samples or free DOX. After incubation for 0.5 and 1 h, respectively, the culture medium was removed and the cells were washed twice with PBS. The cells were fixed with 4% paraformaldehyde, the cytoskeleton was stained with phalloidin-FITC for 1 h, and the cell nuclei were stained with DAPI. Fluorescence images of cells were also obtained with CLSM (Leica, Germany) and analyzed by Leica 2.6.0 software.

Cytotoxicity by MTT Assay: The cytotoxicity of blank and DOX-loaded PVA nanogels was studied by MTT assay using U87-MG cells. Cells were seeded into a 96-well plate at a density of 1×10^4 cells per well in 90 µL of EMEM culture medium containing 10% FBS and incubated at 37 °C with 5% CO_2. After 24 h, 10 µL of blank nanogel samples at different concentrations in PB (10×10^{-3} M, pH 7.4) were added to incubate for another 48 h. To test the cytotoxicity of DOX-loaded nanogels, the cells were first treated with 10 µL of prescribed amounts of DOX-loaded nanogel samples or free DOX for 4 h, and then the medium was replaced by 100 µL of fresh medium for another 48 h incubation. After that, 10 µL of MTT solution (5 mg mL^{-1}) was added, and the cells were incubated for 4 h. The medium was replaced by 150 µL of DMSO to dissolve the resulting purple crystals. The optical densities were measured by a microplate reader at 570 nm. The experiments were conducted in triplicate and the results were presented as the average ± standard deviation.

Blood Circulation and In Vivo Imaging of DOX-Loaded Nanogels: The mice were handled under protocols approved by Soochow University Laboratory Animal Center and the Animal Care and Use Committee of Soochow University (Suzhou, China). 200 µL of DOX-loaded nanogels and free DOX in PB (10×10^{-3} M, pH 7.4, 7.5 mg DOX equiv. kg^{-1}) were intravenously injected into nude mice (18–20 g) via the tail vein ($n = 3$). At prescribed time points postinjection, blood was withdrawn from the eye sockets of nude mice. The blood samples upon withdrawing were immediately dissolved in 0.1 mL of lysis buffer (1% triton X-100) with brief signification. DOX was extracted by incubating blood samples in 0.5 mL of extraction solution (HCl/isopropanal) at –20 °C overnight and followed by centrifugation (14.8 krpm, 30 min). The DOX level in the supernatant was determined by fluorometry.

In order to monitor the fluorescence imaging of nanogel samples in vivo, DIR was loaded into nanogels by hydrophobic interaction with final DIR concentrations of 20 µg mL^{-1}. The U87-MG human glioblastoma tumor xenograft model was established by subcutaneous inoculation of U87-MG cells (1×10^7) in 50 µL of PBS into the right hind flank of each nude mouse (18–20 g). After 20 d, the tumor size reached ≈150–200 mm^3, and the tumor-bearing mice were randomly grouped and injected with DIR-loaded nanogels in 200 µL of PB via tail vein. At predetermined time points (0, 4, 8, 12, 24, and 48 h) post i.v. injection, the mice were anesthetized with isoflurane and during the imaging acquiring process, 3% isoflurane anesthesia was delivered via a nose cone system. The fluorescent images were scanned using a near-infrared fluorescence imaging system (Kodak, Rochester, New York) at excitation of 747 nm and emission of 774 nm, and the images were acquired and analyzed using Lumia II software.

Ex Vivo Imaging and Biodistribution of DOX-Loaded Nanogels: A single dose of DOX-loaded nanogels or free DOX in 200 µL of PBS was administrated intravenously via the tail vein (7.5 mg DOX equiv. kg^{-1}) into nude mice bearing U87-MG tumor xenograft. At 8 h postinjection, the tumor-bearing mice were sacrificed. The tumor blocks and several major organs like heart, liver, spleen, lung, and kidney were collected, washed, dried with paper towel,

and weighed. Fluorescence images were acquired with the Kodak near-infrared fluorescence imaging system.

To quantify the amount of DOX delivered to the tumor and different organs, the tumor block and organs were homogenized in 0.5 mL of 1% triton X-100 with a homogenizer (IKA T25) at 18 000 rpm for 10 min. Each tissue lysate was incubated with 1.0 mL extraction solution (HCl/isopropanal) at −20 °C overnight. After centrifugation (14.8 krpm, 30 min), the DOX in the supernatant was determined by fluorometry based on a calibration curve, and expressed as injected dose per gram of tissue (% ID g^{-1}).

In Vivo Antitumor Efficacy of DOX Loaded Nanogels: Nude mice (18–20 g) were injected subcutaneously in the hind flank with 50 µL of U87-MG cells suspension (1×10^7 cells). Treatment started after 2 weeks when tumors reached 30–50 mm^3, and this day was designated as day 0. The mice were weighed and randomly divided into five groups ($n = 5$): three groups of DOX-loaded different PVA nanogels, free DOX, and PBS. The formulations at a dosage of 7.5 mg DOX equiv. kg^{-1} were i.v. injected via the tail vein every 3 d. The tumor size was measured using calipers every 3 d and tumor volume was calculated according to the formula $V = 0.5 \times L \times W \times H$, wherein L, W, and H were the tumor dimensions at the longest, widest, and highest points, respectively. The relative tumor volume was calculated as V/V_0 (V_0 is the tumor volume at day 0). The relative body weight of the mice was normalized to their initial weight (w/w_0, w_0 is the body weight at day 0). On day 12, the treatment was terminated, and all the mice of each group were sacrificed by cervical vertebra dislocation. The tumor block, heart, liver, and kidney were separated and excised. The tissues were fixed with 4% paraformaldehyde solution and embedded in paraffin. The sliced organ tissues (thickness: 4 mm) mounted on the glass slides were stained by H&E and observed by a digital microscope (Olympus BX41).

Supporting Information

Supporting Information is available from the Wiley Online Library or from the author.

Acknowledgements

W.C. and Y.Z. contributed equally to this work. The authors thank Dr. Florian Mummy (Head of Research & Technical Services in Kuraray Europe GmbH) for providing the PVA samples. The authors also thank Dr. Pamela Winchester for carefully language polishing this manuscript. W.C. thanks the research fellowship from the Alexander von Humboldt Foundation, and Z.Y.Z. thanks the Friedrich Wilhelm Bessel Research Award from the Alexander von Humboldt Foundation.

[1] a) P. Couvreur, *Adv. Drug Delivery Rev.* **2013**, *65*, 21; b) T. Sun, Y. S. Zhang, B. Pang, D. C. Hyun, M. Yang, Y. Xia, *Angew. Chem., Int. Ed.* **2014**, *53*, 12320; c) H. Cabral, K. Kataoka, *J. Controlled Release* **2014**, *190*, 465; d) A. Wicki, D. Witzigmann, V. Balasubramanian, J. Huwyler, *J. Controlled Release* **2015**, *200*, 138; e) M. E. Davis, Z. Chen, D. M. Shin, *Nat. Rev. Drug Discovery* **2008**, *7*, 771; f) T. Wei, C. Chen, J. Liu, C. Liu, P. Posocco, X. Liu, Q. Cheng, S. Huo, Z. Liang, M. Fermeglia, S. Pricl, X. Liang, P. Rocchi, L. Peng, *Proc. Natl. Acad. Sci. USA* **2015**, *112*, 2978; g) M. Talelli, M. Barz, C. Rijcken, F. Kiessling, W. Hennink, T. Lammers, *Nano Today* **2015**, *10*, 93.

[2] a) R. T. Chacko, J. Ventura, J. Zhuang, S. Thayumanavan, *Adv. Drug Delivery Rev.* **2012**, *64*, 836; b) X. Zhang, S. Malhotra, M. Molina, R. Haag, *Chem. Soc. Rev.* **2015**, *44*, 1948; c) A. V. Kabanov, S. V. Vinogradov, *Angew. Chem., Int. Ed.* **2009**, *48*, 5418; d) Y. Tahara, K. Akiyoshi, *Adv. Drug Delivery Rev.* **2015**, *95*, 65; e) Y. Tahara, S.-A. Mukai, S.-I. Sawada, Y. Sasaki, K. Akiyoshi, *Adv. Mater.* **2015**, *27*, 5080; f) Y. Li, D. Maciel, J. Rodrigues, X. Shi, H. Tomás, *Chem. Rev.* **2015**, *115*, 8564; h) L. Zha, B. Banik, F. Alexis, *Soft Matter* **2011**, *7*, 5908.

[3] a) R. Cheng, F. Meng, C. Deng, Z. Zhong, *Nano Today* **2015**, *10*, 656; b) S. Mura, J. Nicolas, P. Couvreur, *Nat. Mater.* **2013**, *12*, 991; c) M. Molina, M. Asadian-Birjand, J. Balach, J. Bergueiro, E. Miceli, M. Calderon, *Chem. Soc. Rev.* **2015**, *44*, 6161.

[4] a) D. Steinhilber, M. Witting, X. Zhang, M. Staegemann, F. Paulus, W. Friess, S. Küchler, R. Haag, *J. Controlled Release* **2013**, *169*, 289; b) J.-H. Ryu, R. T. Chacko, S. Jiwpanich, S. Bickerton, R. P. Babu, S. Thayumanavan, *J. Am. Chem. Soc.* **2010**, *132*, 17227; c) W. Wu, W. Yao, X. Wang, C. Xie, J. Zhang, X. Jiang, *Biomaterials* **2015**, *39*, 260; d) K. Huang, B. Shi, W. Xu, J. Ding, Y. Yang, H. Liu, X. Zhuang, X. Chen, *Acta Biomater.* **2015**, *27*, 179; e) D. Li, N. Kordalivand, M. Fransen, F. Ossendorp, K. Raemdonck, T. Vermonden, W. Hennink, C. van Nostrum, *Adv. Funct. Mater.* **2015**, *25*, 2993; f) J. Li, C. Zheng, S. Cansiz, C. Wu, J. Xu, C. Cui, Y. Liu, W. Hou, Y. Wang, L. Zhang, I. Teng, H. Yang, W. Tan, *J. Am. Chem. Soc.* **2015**, *137*, 1412.

[5] a) R. Cheng, F. Meng, C. Deng, H.-A. Klok, Z. Zhong, *Biomaterials* **2013**, *34*, 3647; b) X. Zhang, K. Achazi, D. Steinhilber, F. Kratz, J. Dernedde, R. Haag, *J. Controlled Release* **2013**, *174*, 209; c) J. Dai, S. Lin, D. Cheng, S. Zou, X. Shuai, *Angew. Chem., Int. Ed.* **2011**, *50*, 9404; d) T. Zhou, X. Zhao, L. Liu, P. Liu, *Nanoscale* **2015**, *7*, 12051; e) Z. Qiao, R. Zhang, F.-S. Du, D.-H. Liang, Z.-C. Li, *J. Controlled Release* **2011**, *152*, 57; f) M. Li, Z. Tang, H. Sun, J. Ding, W. Song, X. Chen, *Polym. Chem.* **2013**, *4*, 1199.

[6] a) M.-H. Alves, B. E. B. Jensen, A. A. A. Smith, A. N. Zelikin, *Macromol. Biosci.* **2011**, *11*, 1293; b) B. V. Slaughter, S. S. Khurshid, O. Z. Fisher, A. Khademhosseini, N. A. Peppas, *Adv. Mater.* **2009**, *21*, 3307; c) H. Geckil, F. Xu, X. Zhang, S. Moon, U. Demirci, *Nanomedicine* **2010**, *5*, 469.

[7] W. Chen, K. Achazi, B. Schade, R. Haag, *J. Controlled Release* **2015**, *205*, 15.

[8] M. Srinivasarao, C. V. Galliford, P. S. Low, *Nat. Rev. Drug Discovery* **2015**, *14*, 203.

[9] a) S. Su, H. Wang, X. Liu, Y. Wu, G. Nie, *Biomaterials* **2013**, *34*, 3523; b) Y. Zhong, F. Meng, C. Deng, Z. Zhong, *Biomacromolecules* **2014**, *15*, 1955; c) V. P. Torchilin, *Nat. Rev. Drug Discovery* **2014**, *13*, 813; d) Y. Miura, T. Takenaka, K. Toh, S. Wu, H. Nishihara, M. R. Kano, Y. Ino, T. Nomoto, Y. Matsumoto, H. Koyama, H. Cabral, N. Nishiyama, K. Kataoka, *ACS Nano* **2013**, *7*, 8583.

[10] Y. Zhong, C. Wang, R. Cheng, L. Cheng, F. Meng, Z. Liu, Z. Zhong, *J. Controlled Release* **2014**, *195*, 63.

[11] J. Li, H. Yang, Y. Zhang, X. Jiang, Y. Guo, S. An, H. Ma, X. He, C. Jiang, *ACS Appl. Mater. Interfaces* **2015**, *7*, 21589.

Received: June 15, 2016
Revised: October 4, 2016
Published online: November 16, 2016

